Characterization of Perylene Diimide Dye Self-Assemblies and Their Use As Templates for the Synthesis of Hybrid and Supermicroporous Nanotubules

Carlos Rodríguez-Abreu,*,[†] Carolina Aubery-Torres,[‡] Conxita Solans,[‡] Arturo López-Quintela,[§] and Gordon J. T. Tiddy[⊥]

[†]International Iberian Nanotechnology Laboratory (INL), Av. Mestre José Veiga, 4715-330 Braga, Portugal

[‡]Instituto de Química Avanzada de Cataluña, Consejo Superior de Investigaciones Científicas (IQAC-CSIC), CIBER-BBN Jordi Girona 18-26, 08034 Barcelona, Spain

[§]Departamento de Química Física, Facultad de Química, Universidad de Santiago de Compostela, 15782 Santiago de Compostela, Spain

[⊥]School of Chemical Engineering and Analytical Science, The University of Manchester, Oxford Road, Manchester, M13 9PL, U.K.

Ⓢ *Supporting Information*

ABSTRACT: The self-organizing structures formed by a water-soluble perylene diimide dye (PDI) have been studied by several experimental techniques as potential templates for the preparation of hybrid nanomaterials. The dye forms chromonic-nematic and hexagonal liquid crystals in water. The aggregates in liquid crystals consist of one-molecule-wide stacks. From the changes in the solution proton NMR chemical shifts with concentration, it appears that adjacent molecules are twisted. There is significant broadening of the aromatic resonances at higher concentrations, arising from nonmotionally averaged dipole—dipole coupling between adjacent aromatic hydrogens. This is attributed to slow overall rotation of the aggregates in solution, suggesting that they grow up to several tens of nanometers. Dye aggregates serve as templates for the formation of silica tubules (1—5 μm length, average diameter ≈300 nm), with aligned and very thin (1—2 nm) dye nanostripes embedded in the walls. The silica tubes precipitated from solution are formed by the cooperative interaction between PDI and silica species during the sol—gel reaction. Upon calcination, silica nanotubules with supermicroporous walls are obtained. In comparison with conventional surfactant systems, the use of π—π stacked chromonic aggregates brings new possibilities for the templated fabrication of pores with sizes below the mesoporous range. Materials could find applications in photovoltaics as well as in shape selective catalysis and adsorption.

KEYWORDS: chromonic liquid crystals, self-assembly, SAXS, NMR, nanostructured silica
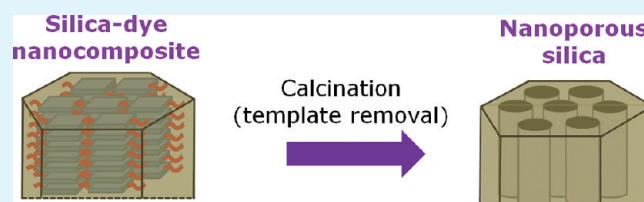
1. INTRODUCTION

Perylene diimide compounds have received much attention in academic and industrial research due to their use as dyes and pigments.[1] They show advantageous properties such as migrational stability, light- and weather-fastness, thermal stability, and chemical inertness as well as high tinctorial strength with a wide range of colors.[2] Perylene diimides are also exceptional n-type semiconductors,[3] having applications in organic field effect transistors,[4] electrophotographic applications, and as molecular components of light-emitting diodes.[5] Moreover, they also show high fluorescence quantum yield and photostability, suitable for applications in the field of laser dyes and fluorescent light collectors.[6,7]

On the other hand, some perylene diimide compounds are capable of self-assembly[8—10] and form thermotropic[11] and chromonic liquid crystal phases in water[12—17] which are characteristic of molecules with disklike or planar shapes that show a strong tendency to aggregate into stacks. Those self-assemblies can, for example, be used to fabricate polarizers[18] or nanofibers.[19,20] Furthermore,

conductive carbon materials can be prepared by pyrolysis of the perylene moiety[21—23]

Although there are some reports on perylene diimide dyes encapsulated in mesoporous silica,[24,25] to our knowledge there is no literature on the direct use of perylene diimide dyes as templates or structure directing agents for the formation of nanostructured oxides. This could enable the preparation of nanocomposites with controlled domain sizes, inorganic—organic heterojunctions, and semiconducting and light-harvesting properties of interest for e.g. photovoltaics. Porous materials with tailored pore size could be also obtained after removing the template.

In this context, we present results on the characterization of self-assemblies in a water-soluble perylene diimide and their use as templates for the preparation of nanostructured silica.
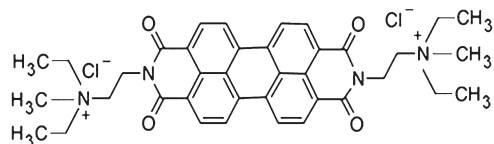
Figure 1. Molecular structure of PDI.

2. EXPERIMENTAL SECTION

2.1. Materials. Bis(N',N'-diethyl-N'-methyl-2-ammoniumethyl)-perylene-3,4,9,-10-tetracarboxylic diimide dichloride, designated herewith as PDI, was synthesized according to the literature.[26] The molecular structure of PDI is shown in Figure.1. Tetraethyl orthosilicate (TEOS) was purchased from Sigma-Aldrich. Ultrapure water (resistivity = 18.2 MΩ/cm) was used in the experiments. All chemicals were used without further purification.

2.2. Methods. *2.2.1. Preparation of PDI Samples in Water.* Mixing of viscous samples at high PDI concentrations was accomplished by repeated centrifugation through the narrow constrictions made in flame-sealed test tubes. Samples with very low concentration were prepared by dilution from more concentrated samples.

2.2.2. Synthesis of Silica. The procedure is similar to one reported in the literature for cationic surfactants.[27] First, a solution of PDI in aqueous ammonia (25%) was prepared. TEOS was added to the solution, and the mixture was stirred for 90 min at 25 °C and then for 90 min at 70 °C. The initial weight ratios for the silica synthesis were typically PDI/NH$_3$(aq)/TEOS = 4/200/40. The obtained precipitate was recovered by filtration and dried. The resulting powder was calcined in air at 600 °C for 6 h (heating rate = 1 °C/min).

2.2.3. Characterization. **2.2.3.1. Microscopy.** Polarized optical microscopy (POM) was performed with a Leica Reichert Polyvar 2. Scanning electron microscopy (SEM) images were taken with a Hitachi TM-1000 and with a Zeiss UltraPlus FESEM instrument. Transmission electron microscopy (TEM) images were collected with a JEOL JEM-2100 microscope at 200 kV(Serveis CientificoTècnics, Universitat de Barcelona, Spain). For TEM observations, samples were embedded in an epoxy resin and then cut in slices about 60 nm thick with a Reichert Jung ultramicrotome.

2.2.3.2. Small Angle X-ray Scattering (SAXS). Small-angle X-ray scattering (SAXS) measurements were performed in an S3MICRO instrument (Hecus X-ray Systems) with point focalization, equipped with a GENIX microfocus X-ray source operating at 50 kV and 1 mA and a FOX2D point-focusing element (both from Xenocs).The scattered intensity was recorded using position-sensitive detectors (Hecus). For the measurements, samples were placed in flame-sealed glass capillaries (diameter = 2 mm). Bragg spacings (d) were calculated from

$$d = 2\pi/q \tag{1}$$

where q is the scattering vector.

For an array of cylinders in a hexagonal lattice, the cylinder diameter (D) can be calculated from

$$D = 2d\left(\frac{2\phi}{\pi\sqrt{3}}\right)^{1/2} \tag{2}$$

Where, ϕ is the volume fraction of cylinders (i.e., aggregates). For the calculation of ϕ, we used a density of 1.3 g/cm^3 for PDI.[28]

2.2.3.3. X-ray Diffraction. X-ray diffraction data were collected with a Philips instrument equipped with a PW1710 control unit, a PW1820/00 vertical goniometer, and an Enraf Nonius FR590 X-ray source.

2.2.3.4. Nuclear Magnetic Resonance (NMR). For ^{2}H NMR spectroscopy, samples were placed in NMR tubes with a diameter of 5 mm. Measurements were recorded at 25 °C using a Bruker DMX-500 NMR
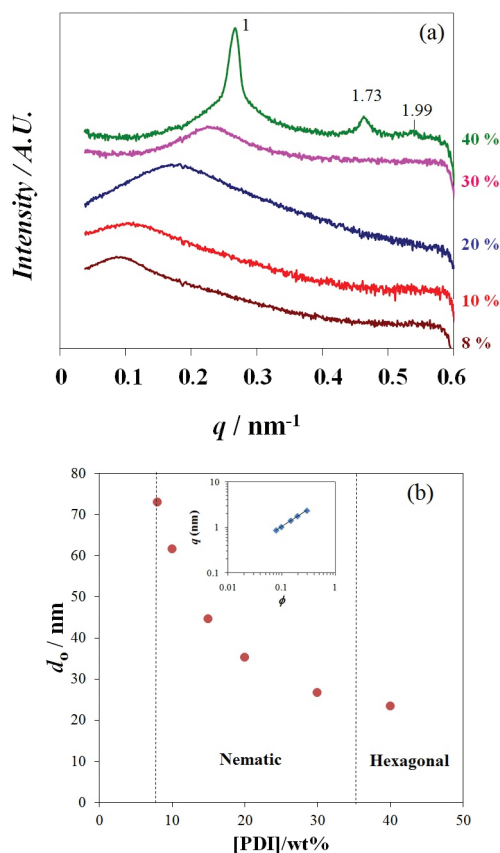

Figure 2. (a) SAXS profiles (25 °C) at different PDI concentrations (in weight percent). The numbers in the uppermost curve indicate the relative positions of reflections (with respect to the first peak). Curves were arbitrarily shifted for clarity of presentation. (b) Bragg spacings from the first X-ray diffraction peak (d_o) at 25 °C as a function of PDI concentration. The inset shows the q vs PDI volume fraction plot in the nematic region.
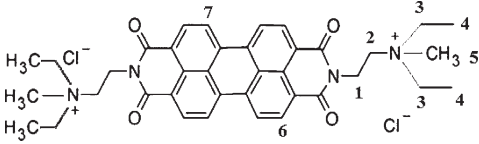
spectrometer (Serveis CientificoTècnics, Universitat de Barcelona). ^{1}H NMR spectra in D$_2$O (4.8 ppm as a reference) were collected at 25 °C on the DPX-400 MHz Bruker instrument of the Manchester Interdisciplinary Biocenter equipped with an autosampler. Variable temperature measurements were made using the Bruker DMX-500 NMR spectrometer. The scan number (NS) of the acquisitions was varied from 100 until 2000 depending on sample concentration.

2.2.3.5. Nitrogen Sorption Isotherms. Nitrogen sorption isotherms were collected with a Micromeritics ASAP 2020 instrument (Unidade de Análise Estructural, SAI, Universidade da Coruña, Spain). Samples were degassed before the measurement. Pore size distributions were calculated with original density functional theory (DFT) using the instrument's software.

3. RESULTS AND DISCUSSION

3.1. Self-Aggregation of PDI. The phase behavior of PDI was already reported by Tam-Chang et al.[26] PDI forms a chromonic-nematic (N) phase from a concentration of about 6 wt %. At higher concentrations, a hexagonal (M) phase was detected. Images of typical optical textures of the studied samples are included in the Supporting Information (Figure S1). At a concentration of 50 wt %, the hexagonal liquid crystal phase coexists with a solid phase. We also confirmed by POM that PDI liquid crystals are formed in aqueous ammonia, which is used for the precipitation of silica, as discussed later.

Table 1. Chemical Shifts As a Function of PDI Concentration

peak assignment	concentration (wt %)						
(relative intensity)	0.005	0.01	0.03	0.1	0.3	0.6	1
1,2 (4)	4.640	4.617	4.630	4.571	4.468	4.374	4.279
3 (4)	3.640	3.641	3.618	3.655	3.648	3.615	3.574
4 (6)	1.542	1.525	1.542	1.550	1.560	1.532	1.494
5 (3)	3.254	3.250	3.251	3.270	3.275	3.243	3.202
6,7 (4)	8.164	8.150	8.137	8.027	7.680	7.465	7.261

SAXS spectra as a function of PDI concentration are shown in Figure 2a. From 8 to 30 wt %, the spectra resemble those observed for some discotic nematic phases,[29] showing a single, relatively broad peak indicative of positional correlations between aggregates. The peak maximum shifts to larger q as concentration is increased, since the distance between aggregates decreases. Within the nematic region, we also found that the full-width at half-maximum of the SAXS peak (estimated from Lorentzian fitting) decreased with concentration, indicating increasing correlation of aggregates along longer distances.[30] Measurements with a 2D detector did not show any preferential alignment of nematic samples inside the capillary. At 40 wt %, the spectrum changes dramatically, now featuring three well resolved peaks with positions at nearly $1:\sqrt{3}:2$ ratios that can be indexed to a hexagonal structure. The 40 wt % sample also showed a peak in the wide angle region, with a maximum at $q = 18.4$ nm^{-1} (see the Supporting Information, Figure S2). This peak is characteristic of chromonic liquid crystals,[31] and it is associated to the separation (along the aggregate's long axis) between the aromatic cores of stacked molecules, i.e. 0.34 nm.

The Bragg spacing from the first, most intense X-ray scattering peak or maximum (d_o) is plotted as a function of PDI concentration in Figure 2b. An increase of d_o with dilution is observed, as liquid crystal phases swells with water and the aggregates separate in direction perpendicular to the long axis. The diameter of aggregates calculated from the interlayer spacing in the M phase at 40 wt % PDI (see eq 2 in the Experimental Section) is 1.7 nm, this value is shorter than the molecular size estimated from bond lengths (~2 nm), which suggests that aggregates are formed by one-molecule-wide stacks. There are several reasons that can explain the difference in the diameter with respect to the molecular size. There might be a deviation from the circular cross section assumed in eq 2. On the other hand, molecules can be tilted. Uncertainties concerning perylene density inside aggregates should also be taken into account.

The q vs PDI concentration plot followed a power law with an exponent (~0.7) higher than that reported (0.5) for semidiluted nematic suspensions of rods;[32] this divergence probably arises from the contribution of the structure factor which reflects the average arrangement of aggregates. Actually, the 0.5 exponent is derived assuming that a hexagonal packing entropy term[33] dominates interparticle correlations within the nematic phase, which may not apply in the present case.
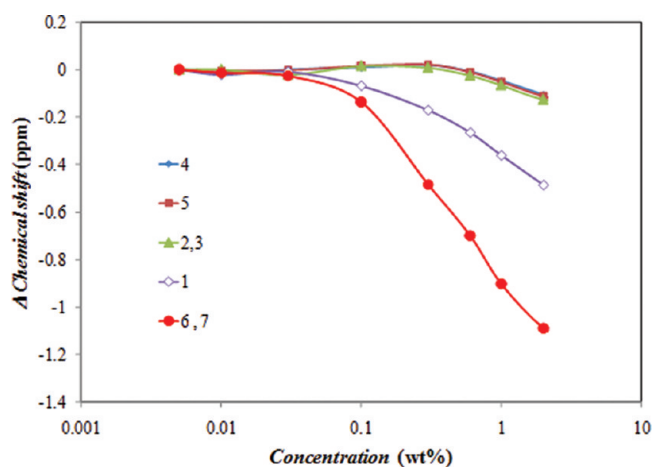
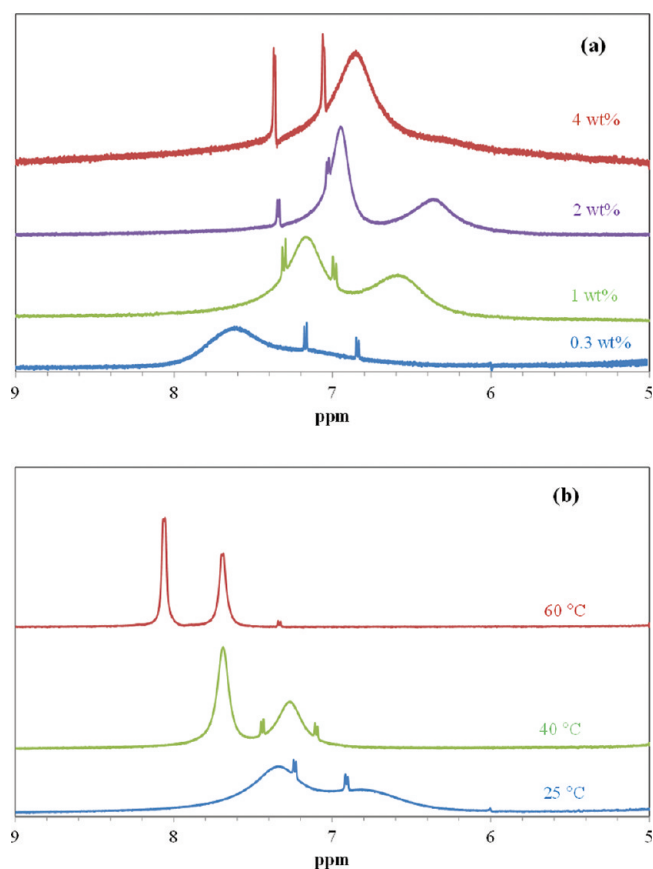**Figure 3.** Relative change in chemical shift at 25 °C of the proton signals as a function of PDI concentration.

Figure 4. ^{1}H NMR spectra of PDI (a) as a function of concentration at 25 °C and (b) as a function of temperature at 1 wt % (The sharp doublets arise from the residual tosylate ions present due to incomplete ion-exchange in the synthesis, see ref 26).

It is well-known that the formation of chromonic aggregates leads to large changes in ^{1}H NMR chemical shifts because of shielding due to the presence of neighboring aromatic rings on adjacent molecules in the stacks ("ring current effect").[34,35] We have measured the chemical shifts (δ-values) for PDI in D$_2$O over a range of concentrations (Table 1). Peak intensities in NMR spectra are proportional to the number of chemically

identical nuclei present in the material; hence, where differing numbers of nuclei occur for different peaks, this is an aid to peak assignment. The relative intensities of the peaks as listed in Table 1 are in agreement with those expected from the chemical structure. At the two lowest concentrations, the signal-to-noise ratio of the spectra is poor (this prevented measurements at even lower concentrations). While the peaks from the nonaromatic hydrogens are sharp (line width at half height <3 Hz), broad resonances are observed at the two lowest concentrations for the aromatic hydrogens (line width ca. 40 Hz). We suspect that this arises from the presence of additional charged species (tricharged) in slow exchange with the dicationic salt. This would influence the aromatic resonances the most because the dicationic salt will have markedly different chemical shifts for these hydrogens. We have not pursued this matter further because of the poor signal-to-noise of the spectra. At higher concentrations the chemical shifts decrease strongly for the aromatic hydrogens (H(6,7), Figure 3). For the other groups, H(1) has about half the change of H(6,7), while the other resonances are scarcely altered. This is exactly what would be expected for self-aggregation into stacks where the aromatic cores lie on top of each other. The monomers exchange rapidly with the aggregates on the NMR timescale (ca. 10^{-2} s), resulting

Table 2. NMR Linewidths for PDI in Water

concentration (wt%)	T (°C)	6 ($\Delta\nu_{1/2}$, Hz)	7 ($\Delta\nu_{1/2}$, Hz)	τ_c (s)
0.3	25	150*	150*	ca. 2×10^{-7}
1	25	120	240	ca. 2×10^{-7}
1	40	43	90	1×10^{-7}
1	60	12	21	1×10^{-9}
2	25	60	120	1.6×10^{-7}
4	25	140	280	6×10^{-7}

*The peaks for H(6) and H(7) overlap; hence, it is not possible to distinguish individual line widths. The number given is for the total line width.

in the occurrence of a single, averaged spectrum. Because of the bulky alkylammonium substituents, it is likely that the rings are aligned at an angle (possibly right angles) to each other.

Figure 4 shows the ^{1}H NMR spectra of PDI as a function of concentration and temperature. As the concentration increases, the aromatic peaks become much broader, and the other peaks also broaden (see Figure 4a). Measurements at two NMR frequencies (400 and 500 MHz) show that this broadening is independent of field strength, so it must arise from nonaveraged dipole—dipole interactions between adjacent protons, as for the line broadening in the chromonic dye Edicol[34] (for the molecular structure of Edicol, see the Supporting Information, Figure S3). We are uncertain of the exact peak assignments for the spectra at low concentrations. But at the higher concentrations, the peak showing the largest shift change is twice as broad as the other peak. This must arise from the hydrogens in the center of the aromatic core which have two nearest neighbor hydrogens, hence twice the dipole—dipole interactions of the peripheral hydrogens, which have one nearest neighbor. To verify the origin of the broad lines, spectra of the 1% sample were obtained for a range of temperatures (see Figure 4b). It is quite clear from the high temperature spectra that the line widths become much narrower, but that the ratio of the two widths at ca. 2:1 is unaltered. On cooling the original spectra reappear. The constant ratio of the two widths at ca. 2:1 supports the mechanism of line broadening as being due to nonaveraged dipole—dipole couplings. Line broadening due to a chemical shift mechanism (chemical exchange) gives broadened peaks with a range of line width ratios.

Note that the chemical shifts for the variable temperature spectra are made with reference to the HOD peak at 4.8 ppm. However, it is well-known that this peak shifts to lower δ values at higher temperatures. Thus, a substantial part of the shift changes with temperature arise from this source. However, if the peaks for H(4) and H(5) are taken to have a temperature invariant chemical shift, then the peaks for H(6) shift to higher values with increasing temperature, by up to 0.5 ppm at 60 °C. This indicates that the aggregates disassociate at higher temperatures.
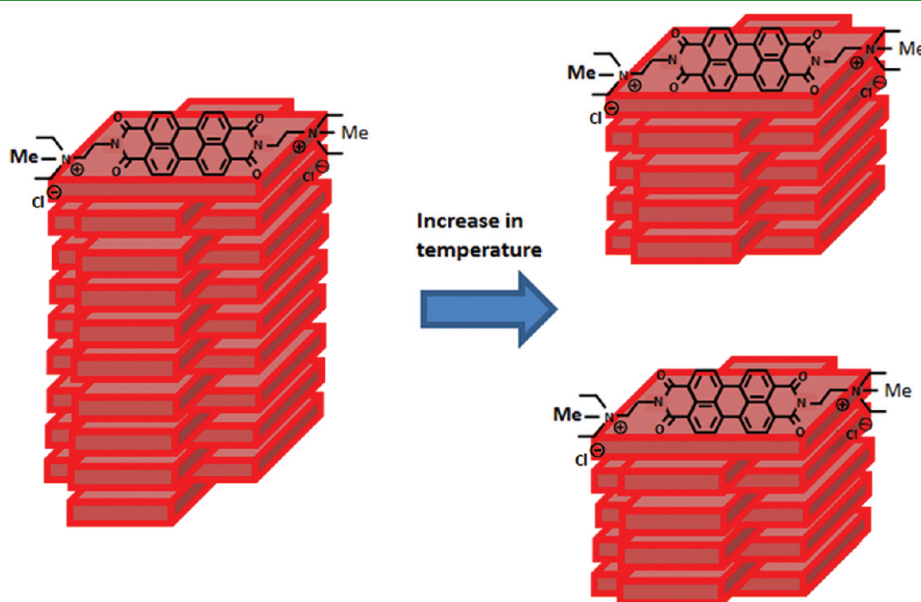
Figure 5. Schematics of the proposed structure for PDI aggregates and how they are affected by temperature.
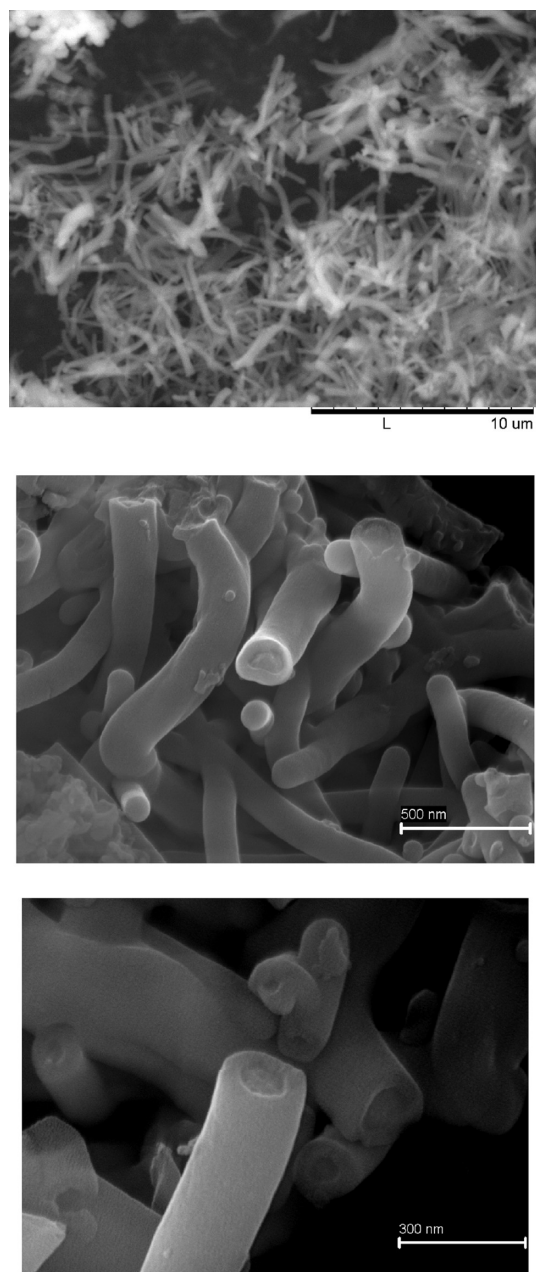
Figure 6. SEM images at different magnifications of calcined silica synthesized from PDI solutions. The initial weight ratios for the silica synthesis were PDI/NH$_3$(aq)/TEOS = 4/200/40.

While we cannot be certain of the shift assignments for H(6), there appears to be a crossover of the chemical shifts at ca. 0.3% concentration. The high-δ peak at <0.3%, (probably from the hydrogens in the center of the aromatic core) shifts to below that of the second peak at high concentrations. Thus, the chemical shift of this peak changes by up to 1.9 ppm at the highest concentration, while the other change is about half of this. This is comparable to the changes seen for Edicol[34] and suggests that almost all of the PDI is in aggregates. Because the changes in the chemical shift with concentration for H(6) appear to be smaller than the changes for H(7), then within the aggregates H(7) must spend significantly more time in close proximity to the aromatic rings of the neighboring molecules than H(6). It has already been

mentioned that the bulky alkylammonium substituents will cause neighboring molecules to be rotated within the aggregates. The different chemical shift changes imply that the rotation angle is quite large. We are unable to specify a value, but a simple examination of the molecular geometry suggests that the angle is >45°. As an additional point, we note that the shift changes for the aromatic hydrogens do not follow exactly the simple two state "monomer/aggregate" model employed for Edicol. This suggests that there is an alteration in the aggregate structure with concentration. Much more detailed NMR data are required for further insights into this phenomenon.

When NMR line widths are determined by ^{1}H dipole—dipole interactions, it is possible to relate the line widths to the correlation time (τ_c) for overall rotation of the aggregates.[34] Because the protons are adjacent to each other, they are in very similar geometries to the protons in Edicol which were employed for size estimations from broadened NMR peaks. We assume that the hydrogens in the center of the aromatic core have twice the dipole—dipole interactions as the peripheral hydrogens. The line widths at half height fall in the range 10—280 Hz, which translate into τ_c values of ca. 1×10^{-9} to 6×10^{-7} s (Table 2). These suggest aggregate lengths of up to several tens of nm. Note that the peak widths for the 2% solution are less than those of the 1% and 4% samples. This indicates nonmonotonic behavior, again requiring further data. The changes in the line widths at 1% over 25—60 °C suggest a significant decrease in rod length with temperature (shown schematically in Figure 6). This is qualitatively similar to other systems such as Edicol.

^{2}H NMR measurements have been carried out for samples of PDI in ^{2}H$_2$O in the nematic phase up to a PDI concentration of 20%. The samples give spectra demonstrating that the mesophase aligns with the director perpendicular to the magnetic field, as expected from the behavior of numerous other chromonic systems. The water quadrupole splittings (Δ) fall in the range 50—200 Hz, again similar to those observed for other systems. They are linearly dependent on the dye/water molar ratio, with the line passing through the origin (see Figure S4 in the Supporting Information). It is well-known that ^{2}H Δ values for water in lyotropic liquid crystalline phases can be described by a simple two-state model involving free and "bound" fractions. There is fast exchange between the two, resulting in a single, averaged spectrum; free water has a zero Δ value, while that of the "bound" state is finite. There are quotation marks around "bound" to show that this water may not be directly bound to the stacks, it simply has a nonzero Δ value because it lies in contact with the stack. The linear dependence of the Δ values on the dye/water molar ratio is good evidence that the structure of the stacks does not change significantly over this concentration range.

The structure of PDI aggregates in solution, determined from the collected experimental evidence, is depicted in Figure 5

3.2. Characterization of Silica Samples. Figure 6 shows SEM images of calcined silica samples prepared from PDI solutions. Cylindrical particles with 1—5 μm length and average diameter ≈300 nm are observed. Some of the particles appear to be hollow. In a previous article,[36] we found that other molecules forming chromonic liquid crystals also direct the formation of elongated silica structures. The formation mechanism is still unclear, but it could be similar to that proposed for organic nanofibers of perylene homologues deposited on substrates,[37] namely, elongated PDI aggregates may associate further to form bundles of larger size; such an association would be promoted by the silica species in solution.
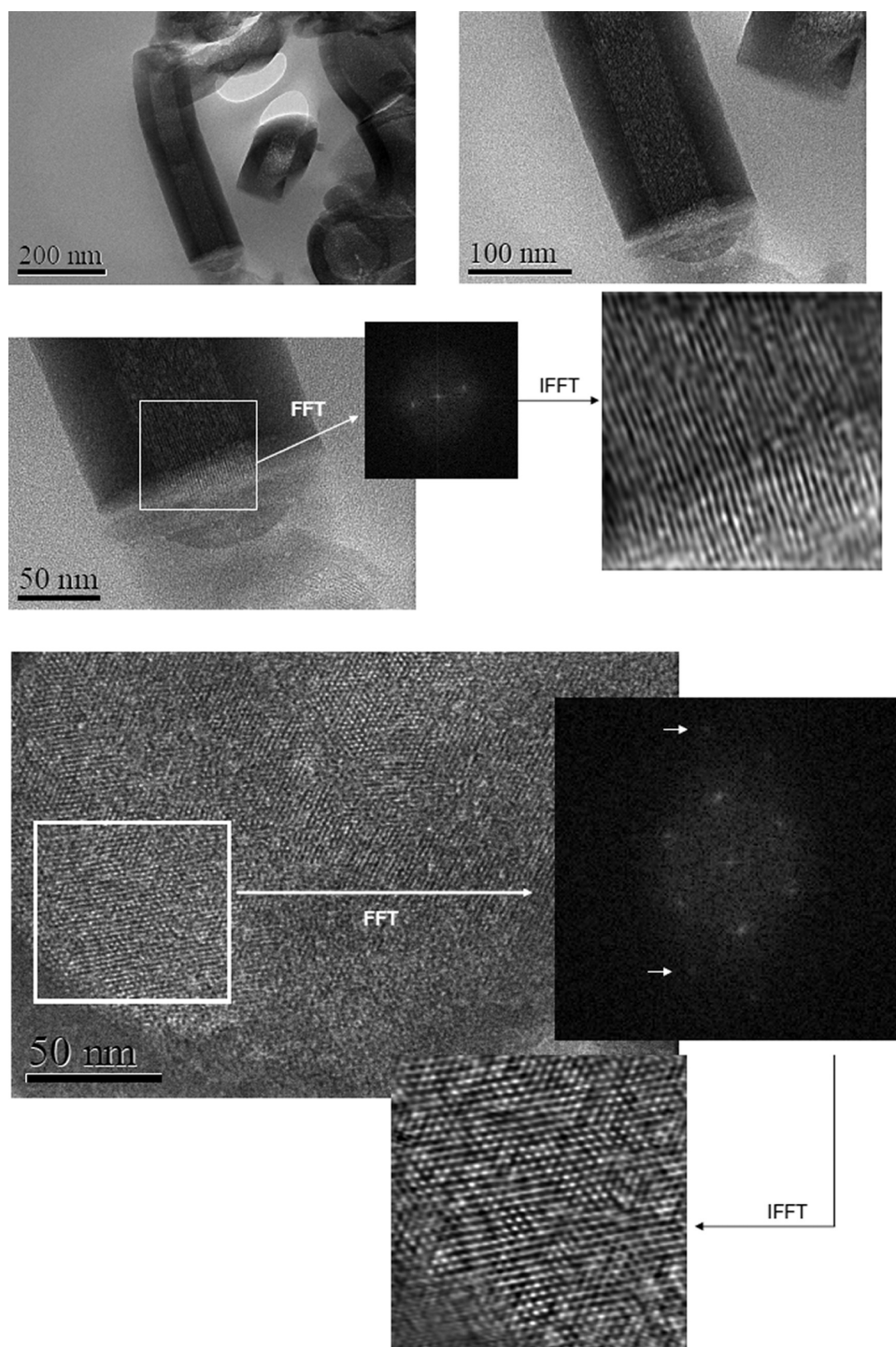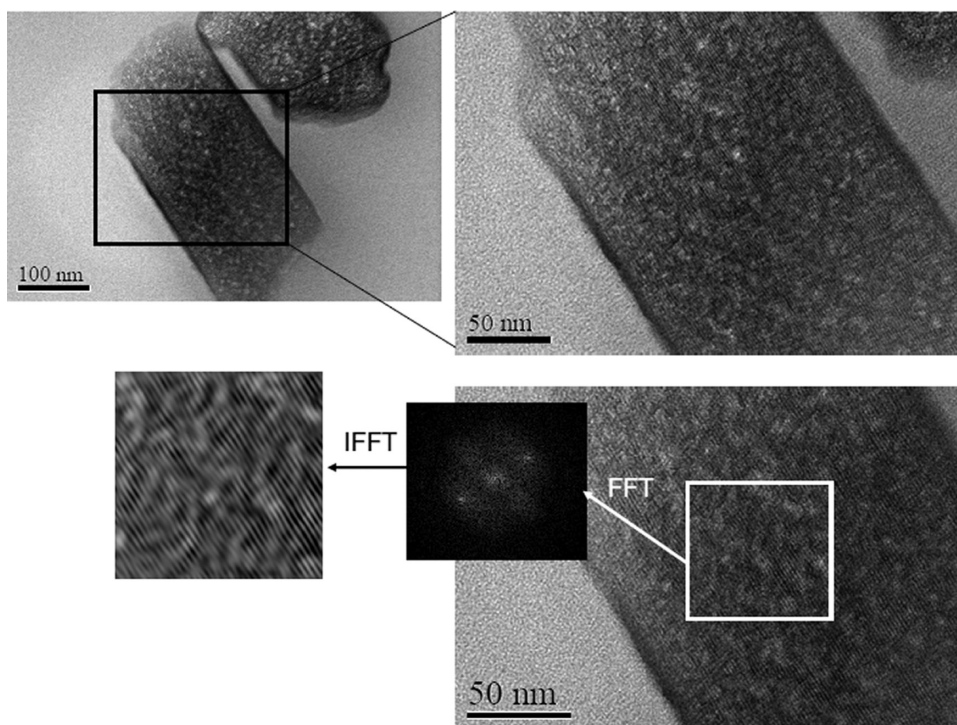
Figure 7. TEM images of noncalcined silica synthesized from PDI solutions. FFT and IFFT stand for Fourier transformation and inverse Fourier transformation of the image, respectively. The initial weight ratios for the silica synthesis were $PDI/NH_3(aq)/TEOS = 4/200/40$.

The hollow nature of silica particles is confirmed by TEM of ultramicrotomed samples (Figure 7). Moreover, images at high magnification of noncalcined samples show the presence of aligned stripes within the particles. The stripes have a width of about 2 nm, i.e. consist of one-molecule-wide rows, and are hexagonally arranged. Therefore, the silica structures resemble the hexagonal liquid crystal found in PDI aqueous solutions, as it occurs in some surfactant systems.[38] Note, however, that the starting composition for the synthesis fall into the isotropic (nonliquid crystalline) region, which suggests that the formation of ordered silica does not take place by direct templating but by precipitation (phase separation) into a more concentrated phase induced by cooperative self-assembly between aggregates and silica species.

Taking into account the properties of PDI, one can assume that the materials contain an array of aligned n-type semiconducting stripes, which could be interesting for electronics and photovoltaic devices. Note that the PDI aggregates can be also

Figure 8. TEM images of calcined silica synthesized from PDI solutions. FFT and IFFT stand for Fourier transformation and inverse Fourier transformation of the image, respectively. The initial weight ratios for the silica synthesis were PDI/NH$_3$(aq)/TEOS = 4/200/40.
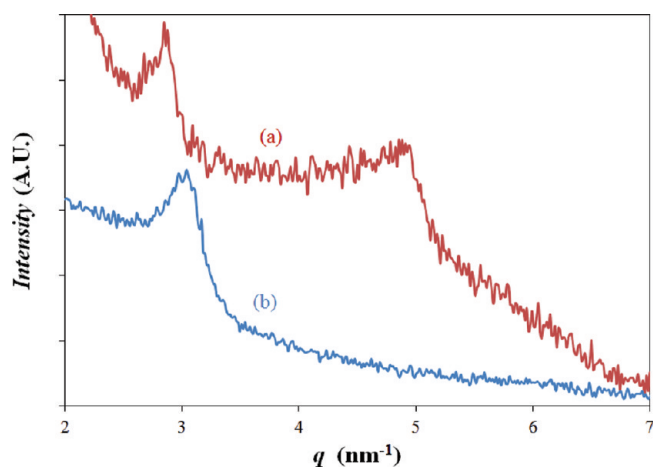
Figure 9. X-ray diffraction curves of silica samples before (a) and after (b) calcination. The initial weight ratios for the silica synthesis were PDI/NH$_3$(aq)/TEOS = 4/200/40.

aligned by shear or by magnetic fields, which could help to increase the size of ordered domains. It is also known that the perylene core can be readily converted into carbon by pyrolysis;[23] therefore, there is a possibility to generate carbon nanowires from the PDI nanostripes.

Figure 8 shows TEM images of samples after calcination. Ordered domains with thin aligned channels (cylindrical pores) were also observed, although they coexisted with some disordered domains. Other sections of the sample (see Figure S5, Supporting Information) showed the presence of cylindrical pores, but not as organized as those observed before calcination. Note that the pores are very narrow (∼1 nm), falling into the supermicroporous range (i.e., with pore diameters between those

of zeolites and mesoporous materials), as they originated after burning out the one-molecule-wide PDI stripes. The synthesis of ordered supermicroporous materials is attractive in the fields of separation and catalysis as well as for applications such as precise molecular recognition, adsorption chemistry, drug delivery, and inclusion chemistry.[39,40] Ordered pores in the range 1.2–2.0 nm would allow shape selective catalysis of organic molecules too large to be accessed by zeolites. While mesoporous materials exhibit great promise in the processing of long-chain and bulky hydrocarbons, in most cases they do not possess enough shape selectivity.[41,42] It is not easy to prepare supermicroporous solids by templating with conventional surfactants as the smallest reachable pore size is limited by the shortest possible chain length for amphiphilic behavior, i.e. the chain length below which the solvophobic effect is not enough to induce the formation of aggregates. Therefore, the present use of $\pi-\pi$ stacked PDI aggregates constitutes a straightforward method to obtain materials with pore size below the mesoporous range.

X-ray diffraction data of silica samples before and after calcination are shown in Figure 9. Two peaks were obtained for the noncalcined sample, with peak position ratios 1:$\sqrt{3}$. They correspond to a hexagonal lattice, in agreement with TEM results. The Bragg spacing corresponding to the first peak in noncalcined samples is 2.2 nm, equivalent to a hexagonal lattice parameter of 2.5 nm. These values are also in agreement with TEM observations and are not much larger than the estimated PDI molecular length (∼2 nm), suggesting that the aggregates would be highly crowded upon silica precipitation, as a result of attractive interaction and cooperative self-assembly with silica species during the sol–gel reaction. After calcination, only one peak is resolved, namely, there is some structure disruption. The absence of high order reflections can also be due to rough or diffuse interfaces,[43,44] which also contributes to peak broadening

4139

dx.doi.org/10.1021/am201016m |*ACS Appl. Mater. Interfaces* 2011, 3, 4133–4141

. Sample contraction as a result of calcination is indicated by the decrease in the Bragg spacing to 2.1 nm.

As no high order reflections were resolved for the calcined samples, there is also the possibility of the structure being pillared or undulated lamellar,[45] although TEM observations correspond more to a framework with cylindrical pores.

Finally, we discuss nitrogen physisorption measurements, shown in the Supporting Information (Figure S6). The isotherm (Figure S6a) is similar to type IV, with a hysteresis loop type H4 associated with narrow, slit-like pores,[46] in which capillary condensation and pore blocking during desorption takes place. The obtained BET surface area was estimated at $249 \pm 1 \ m^2/g$, which is quite similar to that of silica porous nanofibers templated by a cyanine dye.[36] The t-plot method[47] indicated a high fraction of micropores in the sample (corresponding to almost half of the surface area). The pore size distribution calculated by DFT theory (Figure S6b) gives a maximum at 1.3 nm, which agrees approximately with TEM observations and confirms the supermicroporous characteristics of the sample. By subtracting the pore size from the SAXS lattice parameter for a hexagonal structure in the calcined sample (2.4 nm), a wall thickness of 1.1 nm is obtained. If the structure of calcined silica is assumed to be pillared lamellar, the wall thickness would be 0.8 nm.

CONCLUSIONS

The studied PDI dye forms nematic and hexagonal chromonic liquid crystals in water, consisting of stacks of long aggregates with a diameter close to the size of one PDI molecule. NMR results suggest that adjacent molecules are twisted by 90° and that the aggregates in solution grow up to several tens of nanometers.

PDI aggregates interact cooperatively with silica species generated during the sol–gel reaction, hence forming silica particles with tubular shape. Thin PDI stripes (about 2 nm) in a hexagonal arrangement are embedded in the tube walls. Upon calcination, the stripes are burnt off and aligned supermicroporous channels (about 1.3 nm in diameter) are left. Compared to conventional surfactant systems, the use of π–π stacked chromonic aggregates brings new possibilities for the template fabrication of pores with sizes below the mesoporous range. The obtained materials could find applications in photovoltaics as well as in shape selective catalysis and adsorption.

ASSOCIATED CONTENT

ⓢ Supporting Information. Figures S1-S6 as described in the text. This material is available free of charge via the Internet at http://pubs.acs.org.

AUTHOR INFORMATION

Corresponding Author
*E-mail: carlos.rodriguez@inl.int.

ACKNOWLEDGMENT

REFERENCES

(1) Nagao, Y. *Prog. Org. Coat.* **1997**, *31*, 43.

(2) Würthner, F. *Chem. Commun.* **2004**, 1564.

(3) Dimitrakopoulos, C. D.; Malenfant, P. R. L. *Adv. Mater.* **2002**, *14*, 99.

(4) Pron, A.; Gawrys, P.; Zagorska, M.; Djurado, D.; Demadrille, R. *Chem. Soc. Rev.* **2010**, *39*, 2577.

(5) Williams, M. E.; Murray, R. W. *Chem. Mater.* **1998**, *10*, 3603.

(6) Ford, W. E.; Kamat, P. V. *J. Phys. Chem.* **1987**, *91*, 6373.

(7) Bodapati, J. B.; Icil, H. *Dyes Pigments* **2008**, *9*, 224.

(8) Neuteboom, E. E.; Janssen, R. A. J.; Meijer, E. W. *Synth. Met.* **2001**, *121*, 1283.

(9) Balakrishnan, K.; Datar, A.; Naddo, T.; Huang, J.; Oitker, R.; Yen, M.; Zhao, J.; Zang, L. *J. Am. Chem. Soc.* **2006**, *128*, 7390.

(10) Grimsdale, A. C.; Müllen, K. *Angew. Chem., Int. Ed.* **2005**, *44*, 5592.

(11) Nolde, F.; Pisula, W.; Müller, S.; Kohl, C.; Müllen, K. *Chem. Mater.* **2006**, *18*, 3715.

(12) Li, X.-Q.; Zhang, X.; Ghosh, S.; Würthner, F. *Chem.—Eur. J.* **2008**, *14*, 8074.

(13) Tam-Chang, S.-W.; Seo, W.; Iverson, I. K.; Casey, S. M. *Angew. Chem., Int. Ed.* **2003**, *42*, 897.

(14) Huang, L.; Catalano, V. J.; Tam-Chang, S.-W. *Chem. Commun.* **2007**, 2016.

(15) Iverson, I. K.; Tam-Chang, S.-W. *J. Am. Chem. Soc.* **1999**, *121*, 5801.

(16) Tam-Chang, S.-W.; Iverson, I. K.; Helbley, J. *Langmuir* **2004**, *20*, 342.

(17) Naidu, J. J.; Bae, Y.-J.; Jeong, K.-U.; Lee, S. H.; Kang, S.; Lee, M.-H. *Bull. Korean Chem. Soc.* **2009**, *30*, 935.

(18) Huang, L.; Tam-Chang, S.-W.; Seo, W.; Rove, K. *Adv. Mater.* **2007**, *19*, 4149.

(19) Yan, P.; Chowdhury, A.; Holman, M. W.; Adams, D. M. *J. Phys. Chem. B* **2005**, *109*, 724.

(20) Yang, X.; Xu, X.; Ji, H.-F. *J. Phys. Chem. B* **2008**, *112*, 7196.

(21) Rojo, A.; Rosenstratten, A.; Anjo, D. *Anal. Chem.* **1986**, *58*, 2988.

(22) Sayeed, A.; Meenakshi, V.; Bhattacharya, S.; Subramanyam, S. V.; Kanjilal, D. *Vacuum* **1996**, *47*, 1281.

(23) Yi, Z.; Han, X.; Ai, C.; Liang, Y.; Sun, J. *J. Solid State Electrochem.* **2008**, *12*, 1061.

(24) Laerte de Castro, F.; Santos, J. G.; Turolla-Fernandes, G. J.; Souza de Araujo, A.; Fernandes, V. J.; Politi, M. J.; Brochsztain, S. *Micropor. Mesopor. Mater.* **2007**, *102*, 258.

(25) Abdul Wahab, M.; Hussain, H.; He, C. *Langmuir* **2009**, *24*, 4743.

(26) Tam-Chang, S.-W.; Helbley, J.; Iverson, I. K. *Langmuir* **2008**, *24*, 2133.

(27) Di Renzo, F.; Cambon, H.; Dutartre, R. *Microporous Mater.* **1997**, *10*, 283.

(28) Liu, S.-G.; Sui, G.; Cormier, R. A.; Leblanc, R. M.; Gregg, B. A. *J. Phys. Chem. B* **2002**, *106*, 1307.

(29) Mourad, M. C. D.; Byelov, D. V.; Petukhov, A. V.; Matthijs de Winter, D. A.; Verkleij, A. J.; Lekkerkerker, H. N. W. *J. Phys. Chem. B* **2009**, *113*, 11604.

(30) Horowitz, V. R.; Janowitz, L. A.; Modic, A. L.; Heiney, P. A.; Collings, P. J. *Phys. Rev. E* **2005**, *72*, 041710.

(31) Dickinson, A. J.; LaRacuente, N. D.; McKitterick, C. B.; Collings, P. J. *Mol. Cryst. Liq. Cryst.* **2009**, *509*, 9.

(32) Maier, E. E.; Krause, R.; Deggelmann, M.; Hagenbuchle, M.; Weber, R.; Fraden, S. *Macromolecules* **1992**, *25*, 1125.

(33) Odijk, T. *Macromolecules* **1986**, *19*, 2313.

(34) Edwards, D. J.; Jones, J. W.; Lozman, O.; Ormerod, A. P.; Sintyureva, M.; Tiddy, G. J. T. *J. Phys. Chem. B* **2008**, *112*, 14628.

(35) Jones, J. W.; Lue, L.; Ormerod, A. P.; Tiddy, G. J. T. *Liq. Cryst.* **2010**, *37*, 711.

(36) Rodríguez-Abreu, C.; Aubery, C.; Tiddy, G. J. T. *Langmuir* **2011**, *27*, 3067.

(37) Sinks, L. E.; Rybtchinski, B.; Iimura, M.; Jones, B. A.; Goshe, A. J.; Zuo, X.; Tiede, D. M.; Li, X.; Wasielewski, M. R. *Chem. Mater.* **2005**, *17*, 6295.

(38) Takahashi, S.; Ikkai, Y.; Sakamoto, K.; Rodríguez-Abreu, C.; Aramaki, K. *J. Colloid Interface Sci.* **2009**, *335*, 70.

(39) Kato, M.; Shigeno, T.; Kimura, T.; Kuroda, K. *Chem. Mater.* **2005**, *17*, 6416.

(40) Wang, R.; Han, S.; Hou, W.; Sun, L.; Zhao, J.; Wang, Y. *J. Phys. Chem. C* **2007**, *111*, 10955.

(41) Bagshaw, S. A.; Haymanb, A. R. *Chem. Commun.* **2000**, 533.

(42) Corma, A. *Chem. Rev.* **1997**, *97*, 2373.

(43) Rodriguez-Abreu, C.; Esquena, J.; Aramaki, K.; Lopez-Quintela, M. A. *Microporous Mesoporous Mater.* **2009**, *119*, 338.

(44) Melosh, N. A.; Lipic, P.; Bates, F. S.; Wudl, F.; Stucky, G. D.; Frederickson, G. H.; Chmelka, B. F. *Macromolecules* **1999**, *32*, 4332.

(45) Zhou, Y.; Antonietti, M. *Adv. Mater.* **2003**, *15*, 1452.

(46) Sing, K. S. W.; Everett, D. H.; W. Haul, R. A.; Moscou, L.; Pierotti, R. A.; Rouquerol, J.; Siemieniewska, T. *Pure Appl. Chem.* **1985**, *57*, 603.

(47) Lipens, B. C.; Boer, J. H. *J. Catal.* **1965**, *4*, 319.